

RSC Advances



This is an *Accepted Manuscript*, which has been through the Royal Society of Chemistry peer review process and has been accepted for publication.

Accepted Manuscripts are published online shortly after acceptance, before technical editing, formatting and proof reading. Using this free service, authors can make their results available to the community, in citable form, before we publish the edited article. This *Accepted Manuscript* will be replaced by the edited, formatted and paginated article as soon as this is available.

You can find more information about *Accepted Manuscripts* in the [Information for Authors](#).

Please note that technical editing may introduce minor changes to the text and/or graphics, which may alter content. The journal's standard [Terms & Conditions](#) and the [Ethical guidelines](#) still apply. In no event shall the Royal Society of Chemistry be held responsible for any errors or omissions in this *Accepted Manuscript* or any consequences arising from the use of any information it contains.

Pillared clays supported gold catalysts for CO oxidation

Ling Liu, Ying Gao, Pingying Zhao, Xuewen Wang, Gang Feng*, Rongbin Zhang*

Institute of Applied Chemistry, College of Chemistry, Nanchang University, No. 999 Xuefu Road, Nanchang 330031, P. R. China

Abstract: Gold supported on various bentonites were prepared using hydrothermal and co-precipitation methods. The catalysts were characterized by FT-IR, BET, XRD, TEM, SEM, XPS and ICP and tested for CO oxidation reaction. It was found that the Au-Al-Ce pillared bentonite, Au-Al-Ce/Na-LBen(CP) and Au-Al-Ce/Na-LBen(HT), have better catalytic activity and stability than Au/Na-Lben and Au/Al-Ce-Na-LBen. Characterization results show that gold nanoparticle could move into the interlayer spaces of bentonite, which contributes to the high stability of the Au-Al-Ce/Na-LBen(HT) and Au-Al-Ce/Na-LBen(CP) samples. Ce oxide distributes on the surface of Au-Al-Ce/Na-LBen(HT), while stays in the interlayers of the bentonite for the sample Au-Al-Ce/Na-LBen(CP). The pillaring process could increase the $d_{(001)}$ space of the bentonite since the Ce and Au species could move into the interlayer space of the bentonite. The acid-activation process obviously increases the surface area of the bentonite, while the pillaring process increases the surface area of the samples slightly.

Keywords: pillar; bentonite; CO oxidation; gold catalysts; montmorillonite

* Corresponding author. Tel.: +86 136 77080009.

E-mails: fenggang@ncu.edu.cn, Gang Feng; rbzhang@ncu.edu.cn, Rongbin Zhang

1. Introduction

In recent years, gold catalysis has become a hot topic in chemistry.^{1,2} The catalytic activity of supported gold particles was discovered in the 1980s by Masatake Haruta.^{3,4} His pioneering work initiated extensive activities in applied and fundamental researches in this field.⁵ Following the pioneering work of Haruta et al. on the application of supported gold nanoparticles as catalysts for low-temperature CO oxidation, gold catalysts have been widely studied.⁶ The synthesis of gold nanoparticles supported on a variety of metal oxides, such as TiO₂, Fe₂O₃, ZrO₂, CeO₂, Al₂O₃, has been reported.⁷⁻⁹

The catalytic performance of Au is defined by three major factors: contact structure, support selection, and particle size, the first of which being the most important because the perimeter interfaces around Au particles act as the site for reaction.¹⁰ The use of Au as catalysts require careful and unconventional preparation of the Au clusters, focused on achieving very small and stable Au particles (<5 nm).^{3,11,12} The problem is that Au nanoparticles (NPs) could move and aggregate into larger particles on the support surface, which is one of the key issues impeding the application of Au catalysts.¹³⁻¹⁵

Clays are layered oxide materials, which widely exists in nature and could be used as catalyst supports.^{6,16-18} By exchanging the interlayered cations of layered clays with bulky inorganic polyoxocations, followed by calcination, the intercalated polycations increase the basal spacing of the clays and, upon heating, they convert to metal oxide clusters by dehydration and dehydroxylation. In such process the clays became pillared clays. The metal oxide clusters, named pillars, are inserted between the clay layers, yielding temperature stable oxide pillars that permanently keep the layers apart.¹⁸ Previous experiments tried to stabilize metal nanoparticles into the interlayer spaces of clay minerals of the smectite group like montmorillonite, hectorite

and saponite.^{1,2,8,15} Several methods were also reported in the literature for preparation of metal nanoparticles in the interlayer space of modified montmorillonite.^{6,19,20}

As a kind of clay, bentonite has been widely used in many industries as filter materials, decolorant, and adsorbents and so on.^{21,22} The bentonite used as catalyst support remains an important research area, drawing much attention due to its large surface area and moderate reactivity.^{14,15,23-31}

In order to acquire the Au nanoparticles confined in the interlayer space of modified bentonite, the bentonite supported Au-Al-Ce pillaring catalysts were prepared in the present work, and compared with Au nanoparticles catalysts supported on Al-Ce pillared bentonite.^{19,20,25} The catalyst performance was evaluated for the CO oxidation reaction ($2\text{CO} + \text{O}_2 \rightarrow 2\text{CO}_2$), and the catalysts were characterized by FT-IR, BET, XRD, TEM, SEM, XPS and ICP.

2. Experimental

2.1. Preparation of supports and catalyst

The original clay is a commercial type natural bentonite from Jiangxi province, China. It is a calcium montmorillonite, previously separated through a 80 mesh sieve and dipped in deionized water for 24 h. The bentonite was obtained, centrifuged and dried at 70 °C for 12 h. 10 g bentonite was dissolved in 30% (w/w) H₂SO₄ solution at 70 °C for 6 h with the ratio of acid/bentonite(w/w)=5:1. The acid-activated bentonite was centrifuged, washed with deionized water until the pH of the solution became 7, and then dried at 80 °C. The dried acid-activated bentonite was grinded into powders and labeled as LBen. Then sodium bentonite was obtained by dispersing LBen to NaCl aqueous solution with constant stirring at 60 °C for 3 h, until a ratio NaCl/clay(mol/g) = 0.1 was obtained. The clay was then centrifuged and washed with deionized water repeatedly up to the end of chlorides. The bentonite obtained was dried at 80 °C and labeled as Na-Lben.

Al-Ce pillaring solution had been prepared by $\text{AlCl}_3 \cdot 6\text{H}_2\text{O}$ and $\text{Ce}(\text{NO}_3)_3 \cdot 6\text{H}_2\text{O}$, with the Ce/(Al+Ce) molar ratio of 20% and molar concentration for Al^{3+} of 0.5 M. Then the dilute NaOH solution (0.05 M) was added into the mixture slowly until the OH^-/metal molar ratio reaches 2.6. Hydrothermal treatments were carried out in Teflon coated stainless steel pressure vessels, which were slowly rotated for 24 h at 120 °C. Then, the vessels were cooled to room temperature and opened under atmospheric pressure. The mixtures were added drop-wise to Na-LBen slurry (bentonite/water ration of 2g/0.1 L), until the reaction mixture/Na-LBen ratio reaches 20 mmol/g. Then the mixture was stirred continuously for 48 h at 60 °C, after which the mixture was filtered and washed with deionized water until the chlorides were removed. Then, the samples were dried at 80 °C and calcined at 400 °C for 2 h. This sample is labeled as Al-Ce-Na-LBen.

Au/Na-LBen and Au/Al-Ce-Na-LBen catalysts were prepared by deposition-precipitation method with an aqueous of $\text{HAuCl}_4 \cdot 4\text{H}_2\text{O}$ as gold precursor. 1 g of Na-LBen and Al-Ce-Na-LBen were mixed with 10 ml HAuCl_4 solution separately. The suspension was constantly stirred at 70 °C for 2 h, and then 0.5 M NaOH solution was added to the suspension until the pH of the mixture became 8–9. The suspension was then filtered and washed with large amount of deionized water until the chlorides were removed, dried at 80 °C and calcined at 400 °C for 3 h.

Au-Al-Ce pillaring solutions were prepared by co-precipitation method and hydrothermal treatment, respectively. For the co-precipitation method, $\text{AlCl}_3 \cdot 6\text{H}_2\text{O}$, $\text{Ce}(\text{NO}_3)_3 \cdot 6\text{H}_2\text{O}$ and a certain amount of $\text{HAuCl}_4 \cdot 4\text{H}_2\text{O}$ were firstly dissolved into water, with the Al/Ce molar ratios of 20, and the Al^{3+} molar concentration of 0.5 M. A dilute NaOH solution (0.05 M) was added into the suspensions slowly until the ratio of OH^-/metal reaches 2.6. The mixture was stirred at 70 °C for 24 h. Then, the reaction mixture was added drop-wise to Na-LBen slurry (2 g/0.1 L), until the mixture/Na-LBen ratio reaches 20 mmol/g. Then the mixture was stirred continuously for 48 h at

60 °C, filtered, washed with deionized water until the chlorides were removed, dried at 80 °C and calcined at 400 °C for 3 h. This sample is labeled as Au-Al-Ce/Na-LBen(CP). For the hydrothermal treatment, the $\text{AlCl}_3 \cdot 6\text{H}_2\text{O}$, $\text{Ce}(\text{NO}_3)_3 \cdot 6\text{H}_2\text{O}$ and $\text{HAuCl}_4 \cdot 4\text{H}_2\text{O}$ solution and NaOH mixture was kept at 120 °C in Teflon coated stainless steel pressure vessels for 24 h. Then, the mixture was added to the Na-LBen slurry (2 g/0.1 L), until the mixture/Na-LBen ratio reaches 20 mmol/g and stirred for 24 h at room temperature. Then, the products were filtered, washed with deionized water until the chlorides were removed, dried at 80 °C and calcined at 400 °C for 3 h. This sample is labeled as Au-Al-Ce/Na-LBen(HT).

2.2. Catalytic activity tests

The catalysts were evaluated for the CO oxidation reaction with a micro-reactor (stainless steel U-shaped tube, 4 mm i.d.) under atmospheric pressure. The sample (100 mg) is placed among quartz sand. A K-type thermocouple was used to control the reaction temperature. The composition of the feed gas contains 3% CO, 3% O₂ with N₂ as carrier gas and a flow rate of 30 ml/min, which corresponds to a gas hourly space velocity (GHSV) of 18,000 ml/ (g cat·h). The catalyst was reduced in situ under hydrogen flow (30 ml·min⁻¹) at 150 °C for 2 h before the reaction was performed. The reactants and products were analyzed on-line with a GC7890I gas chromatograph equipped with TDX-01 column and TCD with optimized working conditions of carrier gas flow rate at 35~42 mL/ min, column temperature at 80 °C, injector temperature at 100 °C and detector temperature at 110 °C. Before the products analysis, the reaction over the catalysts at each temperature was stabilized for 30 minutes to get steady data.

2.3. Characterization

The contents of the catalysts were analyzed by ICP-AES(optima 5300DV, PE, USA) quantitative analyses (Au line 267.595 Å, plasma power 1200W, plasma flow 1.5 L/min).

XPS characterization was carried out on a PerkinElmer PHI1600 system using a single Mg-K-X-ray source operating at 300 W and 15 kV of voltage. The spectra were obtained at ambient temperature with an ultrahigh vacuum. The binding energies were calibrated using the C 1s peak of graphite at 284.5 eV as a reference.

XRD analyses were performed on a Bruker AXS D8Focus diffract meter instrument operated at 40 kV and 40 mA with Cu target $K\alpha$ -ray irradiation. Scans were collected over a range of 2θ from 2° to 90° with a speed of $2^\circ/\text{min}$.

The specific surface area, pore volume, and average pore diameter of the supports and catalysts were measured by BET methods using a Micromeritics ASAP2020C instrument. Before analysis, the samples were degassed for 1h at 90°C and 10h at 200°C in vacuum.

The morphologies of the samples were investigated by scanning electron microscopy (SEM, FEI Quanta 200F).

Transmission and high resolution transmission electron microscopic images were obtained on a JEOL JSM-2010 electron microscope. The powders were suspended in ethanol for about 10 min under ultrasonic treatment before been deposited on carbon-film-coated copper grids. The average gold particle diameter and its distribution were determined by counting more than 50 particles.

FT-IR spectral data (KBr pellets) were collected in the range of $400\text{-}4000\text{cm}^{-1}$ on VARIAN 2000 FT-IR.

3. Results and discussion

3.1. Characterization

3.1.1 ICP and XPS

The compositions of Au and Ce of the catalysts were characterized by ICP and XPS, and the results are shown in Table 1. For Au-Al-Ce/Na-LBen(CP), Au-Al-Ce/Na-LBen(HT) and Au/Al-

Ce-Na-LBen, the real surface contents of Au characterized by XPS are less than that of ICP. It indicates that part of the Au nanoparticles has gone into the inter-layers of the bentonite. In addition, it is found the XPS results show that the surface contents of Ce in Au-Al-Ce/Na-LBen(CP) is 0, v.s. 6.14% for the Au-Al-Ce/Na-LBen(HT) sample. It suggests that Ce distributes on the surface of Au-Al-Ce/Na-LBen(HT). While, for Au-Al-Ce/Na-LBen(CP), Ce stays in the interlayers of the bentonite.

3.1.2 XRD and BET

X-ray diffraction was used to characterize the structures of the samples. XRD diagrams between 2° and 90° (2θ) of Au/Al-Ce-Na-LBen, Au/Na-LBen, Au-Al-Ce/Na-LBen(HT) and Au-Al-Ce/Na-LBen(CP) are presented in Fig. 3. 2θ angles at about 19.88 and 26.78 belong to kaolinite and SiO_2 , respectively.³² It can be seen that the $d_{(001)}$ spacing of Na-LBen is 12.35 Å, while the $d_{(001)}$ spacings of Au-Al-Ce/Na-LBen(HT) and Au-Al-Ce/Na-LBen(CP) are 14.19 Å and 14.04 Å respectively. Shifting of 2θ valuing from 7.350 to 6.290 clearly suggests expansion of clay layers during preparation. The $d_{(001)}$ spacing increased from 12.35 Å (Na-LBen) to 12.51 Å for Au/Al-Ce-Na-LBen in the present case, indicating the presence of ion substituted Al-Ce pillaring solution as polymers. These sentences should be rewritten. In addition, it is found that the XRD diagrams of Au-Al-Ce/Na-LBen(CP) and Au-Al-Ce/Na-LBen(HT) show strong peaks of CeO_2 . On the contrary, the Au/Al-Ce-Na-LBen sample does not show the CeO_2 peak. It indicates that the Ce aggregated into larger particles in Au-Al-Ce/Na-LBen(CP) and Au-Al-Ce/Na-LBen(HT), while Ce was highly dispersed in Au/Al-Ce-Na-LBen.

BET surface area, average pore volume, and average pore diameter for all the samples are shown in Table 2. It shows that the original Ben had a BET surface area of 35.5 m^2/g , after the acid-activation, the LBen became 210.9 m^2/g , it indicates the acid-activation process could increase the BET surfaces of the bentonite. While, direct ion-exchange process could reduce the

BET surface areas of the samples, as indicated by the BET surface area of Ben and LBen (35.5 and 210.9) v.s. Na-Ben and Na-LBen (32.8 and 153.8 m²/g). In addition, it is found that the BET surface area of Na-LBen increases from 153.8 to 187.3 m²/g for Au-Al-Ce/Na-LBen(CP). It indicates that the pillaring process increases the BET surface area of the samples,³³ since the process creates regular porosity. However, the surface area of Al-Ce-Na-Lben decreased from 179.7 to 168.1 m²/g for Au/Al-Ce-Na-LBen. This may be because some of the Au nanoparticles go into the interlayers of the bentonite.

3.1.3 TEM and SEM

The TEM images of Au-Al-Ce/Na-LBen(CP) and Au/Al-Ce-Na-LBen are depicted in Fig. 4. It shows that bentonite has a layered structure and a two-dimension porous structure with small basal spacing. For Na-LBen the layers are obviously kept apart, obtaining large pore structures and the large $d_{(001)}$ spacing. It is reported that the intercalated polycations increase the basal spacing of the clays and, upon heating they are converted to metal oxide clusters by dehydration and dehydroxylation processes. These metal oxide clusters (pillars) between clay layers permanently keep apart the layers, generating an interlayer space of molecular dimensions.^{15,29} Fig. 4(a) and 4(b) show that both Au-Al-Ce pillaring species and Au nanoparticles appeared as particles, in the diameter of 5–19 and 1–4 nm respectively. In addition, for the Au/Al-Ce-Na-LBen, some of the Au nanoparticles entered the interlayers of bentonite. For the Au-Al-Ce/Na-LBen(CP), the Au-Al-Ce pillaring species homogeneously dispersed in the interlayers of bentonite.

SEM micrographs of Au-Al-Ce/Na-LBen(CP) and Au/Al-Ce-Na-LBen are illustrated in Fig. 5. It is shown that the Au-Al-Ce/Na-LBen(CP) sample has a uniform particles size. While, the particle sizes of Au/Al-Ce-Na-LBen are irregular.

3.1.4 FT-IR

The FT-IR spectra of Al-Ce-Na-Lben, Na-Lben, Au-Al-Ce/Na-LBen(CP), Au-Al-Ce/Na-LBen(HT), Au/Na-Lben and Au/Al-Ce-Na-LBen are shown in Fig. 6. The spectrum of Na-LBen showed the characteristic bands in the range of 3300–3800 cm^{-1} presents the interlayer H-bonded O–H, 1623 cm^{-1} (H–O–H bending), 1037 cm^{-1} , 1098 cm^{-1} (Si–O stretching), 521 and 465 cm^{-1} (Si–O–Si and Si–O–Al deformation vibrations, respectively).²⁴ Meanwhile, compared with pure Na-LBen, the characteristic peaks of other samples have some changes, due to the interactions between the supports and nanoparticles.

3.2. Catalytic activity and stability tests

The selectivity of the CO oxidation to CO_2 is 100%. The yield of CO_2 is equal to the CO conversion. The catalytic performances of the prepared catalysts for CO oxidation are shown in Fig. 1. It should be mentioned that the clay without gold does not show any catalytic activity for the CO oxidation. Our results show that the activity of Au catalysts for CO oxidation highly depends on the type of supports and the preparation methods. In addition, the CO conversion increases as the temperature rises at low temperature. Fig. 1 shows that Au/Na-LBen acquires its best performance until the temperature reaches 330 °C. Au/Al-Ce-Na-LBen acquires its best performance until the temperature reaches 310 °C. Au-Al-Ce/Na-LBen(CP) could reach its best performance at 200 °C (the turnover number of the CO oxidation over Au-Al-Ce/Na-LBen(CP) catalyst is $2.15 \times 10^{16}/\text{s} \cdot \text{m}^2$ for 100% CO conversion.), v.s. 240 °C for Au-Al-Ce/Na-LBen(HT) and 310 °C for Au/Al-Ce-Na-LBen. It indicates that Au-Al-Ce pillaring species and the co-precipitation method contribute to the high CO conversion activity of the catalysts.

Some experiments reported that the gold nanoparticles could catalyze the CO oxidation reaction at lower temperature.^{4,9,34} It should be noted that the catalytic performance of Au is defined by three major factors¹⁰: contact structure, support selection, and particle size, the first of which being the most important because the perimeter interfaces around Au particles act as the

site for reaction. The sizes of the gold particles of the Au-Al-Ce/Na-LBen(CP) catalyst are as small as the reported work, while the contact structure and support interaction are different, which may contribute to the activity of the catalyst.

Except for the activity, the stability of the catalyst is another important factor to evaluate the catalytic performance. Fig. 2 shows the durability tests of CO oxidation for the Au-Al-Ce/Na-LBen(CP) and Au/Al-Ce-Na-LBen. The reaction temperature for Au-Al-Ce/Na-LBen(CP) and Au/Al-Ce-Na-LBen are 170 °C and 290 °C, respectively, which obtained ~80% CO conversions. Fig. 2 shows that no obvious deactivation was observed for the Au-Al-Ce/Na-LBen(CP) catalyst during the 60 h's evaluation. While, the CO conversion over the Au/Al-Ce-Na-LBen decreases from 80% to 60% in 60 h's evaluation. It indicates that the Au-Al-Ce/Na-LBen(CP) shows much better stability than Au/Al-Ce-Na-LBen.

Furthermore, we tried to stop the CO oxidation reaction over the Au-Al-Ce/Na-LBen(CP) catalyst and restart the reaction after the reactor was cooled to room temperature. It shows that Au-Al-Ce/Na-LBen(CP) catalyst could perform as well as the first run.

4. Conclusions

Au/Na-Lben, Au-Al-Ce/Na-LBen(HT), Au-Al-Ce/Na-LBen(CP) and Au/Al-Ce-Na-LBen catalysts are synthesized using hydrothermal and co-precipitation methods for CO oxidation reaction. It is found that Au-Al-Ce/Na-LBen(CP) and Au-Al-Ce/Na-LBen(HT) have better catalytic activity and stability than Au/Na-Lben and Au/Al-Ce-Na-LBen. The samples were characterized using XPS, XRD, BET, TEM, SEM and FT-IR. XPS analysis found that Ce oxide distributes on the surface of Au-Al-Ce/Na-LBen(HT), while stays in the interlayers of the bentonite for the sample Au-Al-Ce/Na-LBen(CP). In addition, the gold nanoparticle could move into the interlayer spaces of bentonite, which contributes to the high stability of the Au-Al-

Ce/Na-LBen(HT), Au-Al-Ce/Na-LBen(CP) samples. The XRD characterization indicates that the pillaring process could increase the $d_{(001)}$ space of the bentonite since the Ce and Au species could move into the interlayer space of the bentonite. The BET results show that the acid-activation process obviously increases the surface area of the bentonite, while the pillaring process increases the surface area of the samples slightly. The TEM results indicate that the Au-Al-Ce pillaring species homogeneously dispersed in the interlayer of bentonite for Au-Al-Ce/Na-LBen(CP). SEM micrograph shows that the Au-Al-Ce/Na-LBen(CP) sample has a uniform particles size, while, the particle sizes of Au/Al-Ce-Na-LBen(24h) are irregular. The FTIR results show that, compared with Na-LBen, some new peaks emerged for the samples with Au, due to the interaction between the supports and nanoparticles.

Acknowledgement

We thank the National Natural Science Foundation of China (21166018) and the Education Department of Jiangxi Province of China (GJJ10291, GJJ14121) for their financial support.

References

- 1 A. A. Teixeira-Neto, B. Faceto, L. S. Siebra, and E. Teixeira-Neto, Effect of the Synthesis Method on the Properties and Catalytic Activities of Au/Pd Nanoparticles Supported on Organophilic Clay, *Appl. Clay Sci.*, 2015, **116**, 175-81.
- 2 B. J. Borah, D. Dutta, and D. K. Dutta, Controlled Nanopore Formation and Stabilization of Gold Nanocrystals in Acid-Activated Montmorillonite, *Appl. Clay Sci.*, 2010, **49**, 317-23.

- 3 M. Haruta, N. Yamada, T. Kobayashi, and S. Iijima, Gold Catalysts Prepared by Coprecipitation for Low-Temperature Oxidation of Hydrogen and of Carbon Monoxide, *J. Catal.*, 1989, **115**, 301-09.
- 4 Masatake Haruta, Tetsuhiko Kobayashi, Hiroshi Sano, and Nobumasa Yamada, Novel Gold Catalysts for the Oxidation of Carbon Monoxide at a Temperature Far Below 0 °C, *Chem. Lett.*, 1987, **16**, 405-08.
- 5 M. Haruta, and M. Date, Advances in the Catalysis of Au Nanoparticles, *Appl. Catal., A*, 2001, **222**, 427-37.
- 6 L. H. Zhu, S. Letaief, Y. Liu, F. Gervais, and C. Detellier, Clay Mineral-Supported Gold Nanoparticles, *Appl. Clay Sci.*, 2009, **43**, 439-46.
- 7 X. He, L. J. Fu, and H. M. Yang, Insight into the Nature of Au-Au₂O₃ Functionalized Palygorskite, *Appl. Clay Sci.*, 2014, **100**, 118-22.
- 8 L. F. Chen, J. C. Hu, and R. Richards, Intercalation of Aggregation-Free and Well-Dispersed Gold Nanoparticles into the Walls of Mesoporous Silica as a Robust "Green" Catalyst for N-Alkane Oxidation, *J. Am. Chem. Soc.*, 2009, **131**, 914-+.
- 9 M. Haruta, S. Tsubota, T. Kobayashi, H. Kageyama, M. J. Genet, and B. Delmon, Low-Temperature Oxidation of Co over Gold Supported on TiO₂, α -Fe₂O₃, and Co₃O₄, *J. Catal.*, 1993, **144**, 175-92.
- 10 M. Haruta, Catalysis of Gold Nanoparticles Deposited on Metal Oxides, *CATTECH*, 2002, **6**, 102-15.
- 11 Y. T. Yu, Q. H. Zhang, and B. Q. Xu, Shape-Controlled Syntheses of Metal Nanoparticles, *Prog Chem*, 2004, **16**, 520-27.
- 12 M. Haruta, Size- and Support-Dependency in the Catalysis of Gold, *Catal. Today*, 1997, **36**, 153-66.

- 13 Y. Zhang, X. J. Cui, F. Shi, and Y. Q. Deng, Nano-Gold Catalysis in Fine Chemical Synthesis, *Chem. Rev.*, 2012, **112**, 2467-505.
- 14 C. C. Chen, and P. L. Kuo, Gold Nanoparticles Prepared Using Polyethylenimine Adsorbed onto Montmorillonite, *J. Colloid Interface Sci.*, 2006, **293**, 101-07.
- 15 T. J. Pinnavaia, S. D. Landau, M. S. Tzou, I. D. Johnson, and M. Lipsicas, Layer Cross-Linking in Pillared Clays, *J. Am. Chem. Soc.*, 1985, **107**, 7222-24.
- 16 A. Alvarez, S. Moreno, R. Molina, S. Ivanova, M. A. Centeno, and J. A. Odriozola, Gold Supported on Pillared Clays for Co Oxidation Reaction: Effect of the Clay Aggregate Size, *Appl. Clay Sci.*, 2012, **69**, 22-29.
- 17 A. Gil, S. A. Korili, R. Trujillano, and M. A. Vicente, A Review on Characterization of Pillared Clays by Specific Techniques, *Appl. Clay Sci.*, 2011, **53**, 97-105.
- 18 A. Gil, L. M. Gandia, and M. A. Vicente, Recent Advances in the Synthesis and Catalytic Applications of Pillared Clays, *Catal. Rev.-Sci. Eng.*, 2000, **42**, 145-212.
- 19 N. R. Sanabria, M. A. Centeno, R. Molina, and S. Moreno, Pillared Clays with Al-Fe and Al-Ce-Fe in Concentrated Medium: Synthesis and Catalytic Activity, *Appl. Catal., A*, 2009, **356**, 243-49.
- 20 J. G. Carriazo, R. Molina, and S. Moreno, A Study on Al and Al-Ce-Fe Pillaring Species and Their Catalytic Potential as They Are Supported on a Bentonite, *Appl. Catal., A*, 2008, **334**, 168-72.
- 21 M. Nafees, and A. Waseem, Organoclays as Sorbent Material for Phenolic Compounds: A Review, *Clean-Soil Air Water*, 2014, **42**, 1500-08.
- 22 A. R. Razakamanantsoa, G. Barast, and I. Djeran-maigre, Hydraulic Performance of Activated Calcium Bentonite Treated by Polyionic Charged Polymer, *Appl. Clay Sci.*, 2012, **59-60**, 103-14.

- 23 A. Khenifi, B. Zohra, B. Kahina, H. Houari, and D. Zoubir, Removal of 2,4-Dcp from Wastewater by Ctab/Bentonite Using One-Step and Two-Step Methods: A Comparative Study, *Chem. Eng. J.*, 2009, **146**, 345-54.
- 24 Z. L. Mo, P. Zhang, D. D. Zuo, Y. L. Sun, and H. Chen, Synthesis and Characterization of Polyaniline Nanorods/Ce(OH)₃-Pr₂O₃/Montmorillonite Composites through Reverse Micelle Template, *Mater. Res. Bull.*, 2008, **43**, 1664-69.
- 25 S. F. Zuo, and R. X. Zhou, Al-Pillared Clays Supported Rare Earths and Palladium Catalysts for Deep Oxidation of Low Concentration of Benzene, *Appl. Surf. Sci.*, 2006, **253**, 2508-14.
- 26 Shaojun Yao, Shuai Yuan, Junhui Xu, Ying Wang, Jianlin Luo, and Shengshui Hu, A Hydrogen Peroxide Sensor Based on Colloidal MnO₂/Na-Montmorillonite, *Appl. Clay Sci.*, 2006, **33**, 35-42.
- 27 Jiyun Feng, Raymond S. K. Wong, Xijun Hu, and Po Lock Yue, Discoloration and Mineralization of Orange Ii by Using Fe³⁺-Doped TiO₂ and Bentonite Clay-Based Fe Nanocatalysts, *Catal. Today*, 2004, **98**, 441-46.
- 28 A. Phukan, J. N. Ganguli, and D. K. Dutta, ZnCl₂-Zn²⁺-Montmorillonite Composite: Efficient Solid Acid Catalyst for Benzylation of Benzene, *J. Mol. Catal. A: Chem.*, 2003, **202**, 279-87.
- 29 L. M. Gandía, M. A. Vicente, and A. Gil, Preparation and Characterization of Manganese Oxide Catalysts Supported on Alumina and Zirconia-Pillared Clays, *Appl. Catal., A*, 2000, **196**, 281-92.
- 30 K. Bahranowski, and E. M. Serwicka, ESR Study of Vanadium-Doped Alumina- and Titania-Pillared Montmorillonites, *Colloid Surface A*, 1993, **72**, 153-60.

- 31 R. M. Barrer, and D. M. MacLeod, Activation of Montmorillonite by Ion Exchange and Sorption Complexes of Tetra-Alkyl Ammonium Montmorillonites, *Transactions of the Faraday Society*, 1955, **51**, 1290-300.
- 32 S. F. Zuo, Q. Q. Huang, and R. X. Zhou, Al/Ce Pillared Clays with High Surface Area and Large Pore: Synthesis, Characterization and Supported Palladium Catalysts for Deep Oxidation of Benzene, *Catal. Today*, 2008, **139**, 88-93.
- 33 E. Booij, J. T. Kloprogge, and J. A. R. vanVeen, Large Pore Ree/Al Pillared Bentonites: Preparation, Structural Aspects and Catalytic Properties, *Appl. Clay Sci.*, 1996, **11**, 155-62.
- 34 B. L. Moroz, P. A. Pyrjaev, V. I. Zaikovskii, and V. I. Bukhtiyarov, Nanodispersed Au/Al₂O₃ Catalysts for Low-Temperature Co Oxidation: Results of Research Activity at the Boreskov Institute of Catalysis, *Catal. Today*, 2009, **144**, 292-305.

Fig.1. Reaction performance of the catalysts for CO oxidation

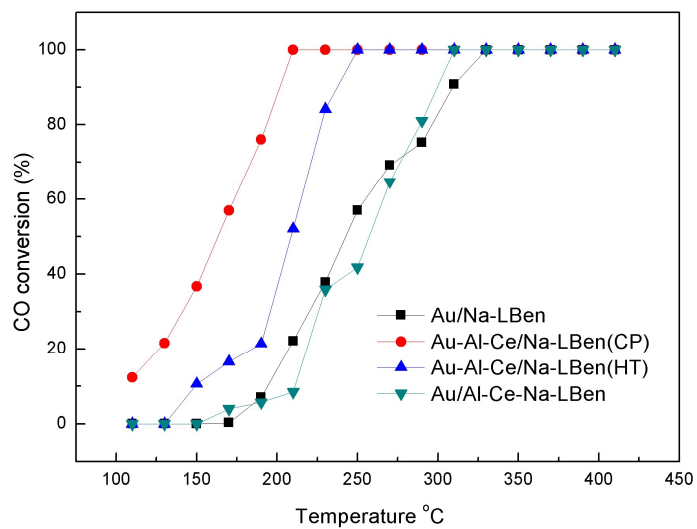


Fig. 2. Time-on-stream evolution of the catalyst for CO conversion

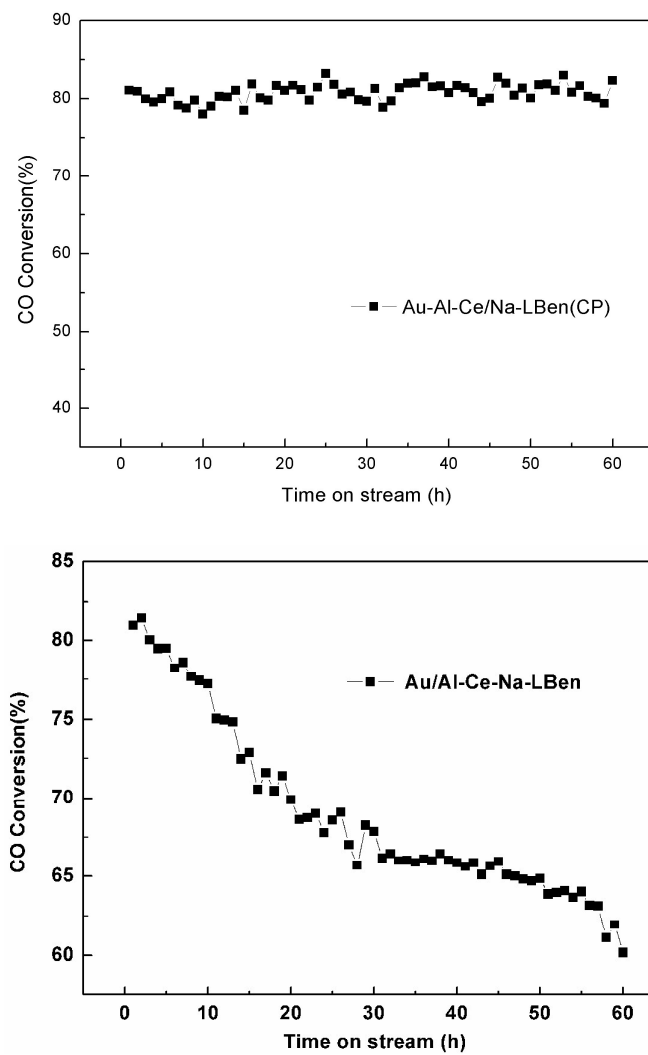


Fig. 3. XRD patterns of the catalysts. a. Au/Al-Ce-Na-LBen, b. Au/Na-LBen, c. Au-Al-Ce/Na-LBen(HT), d. Au-Al-Ce/Na-LBen(CP)

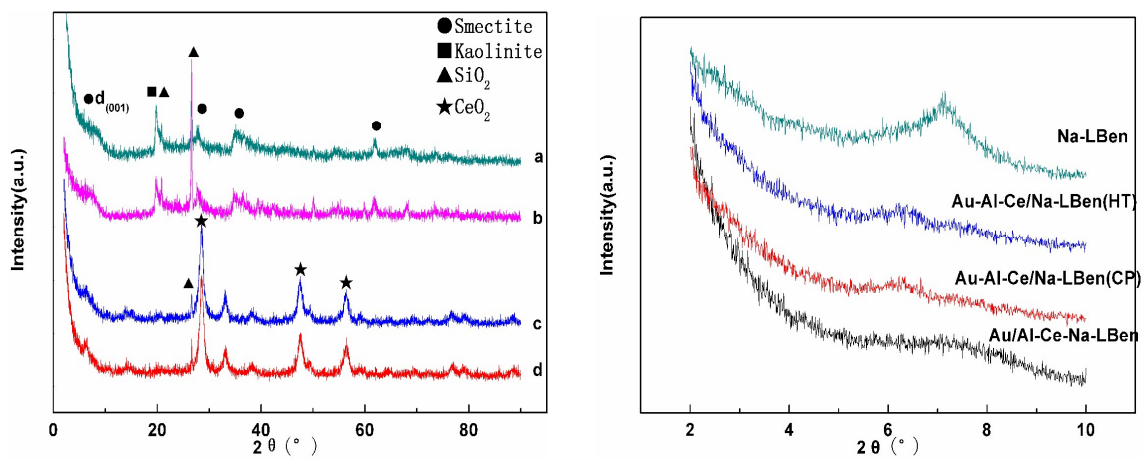


Fig. 4. TEM images of the catalysts (a) and (c) Au-Al-Ce/Na-LBen(CP) (b) and (d) Au/Al-Ce-Na-LBen

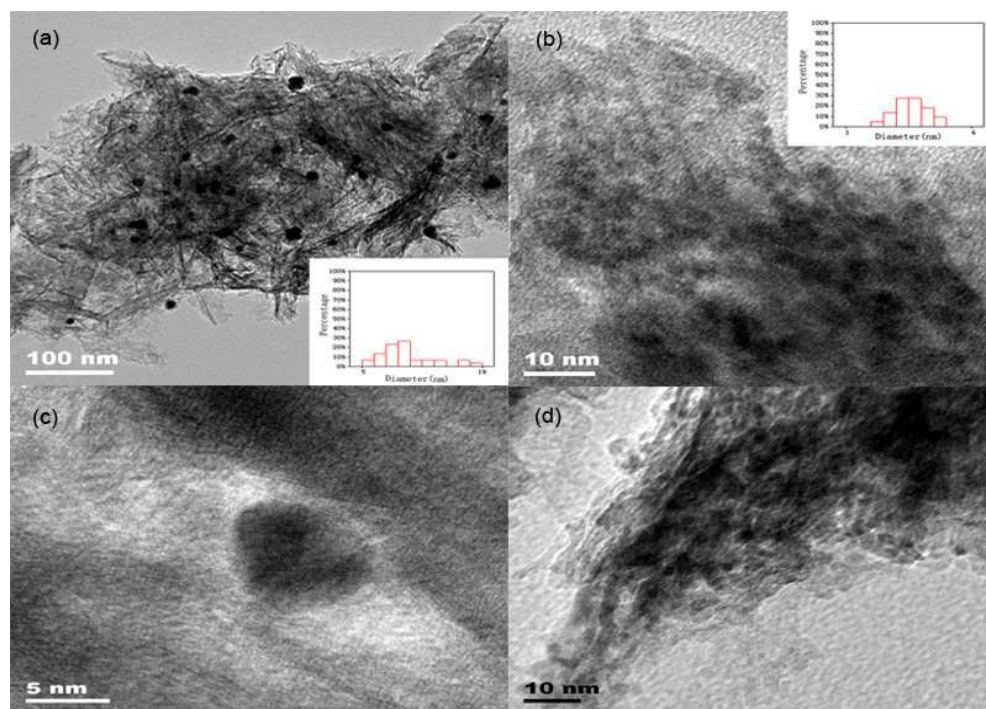


Fig. 5. SEM images of the catalysts (a) Au-Al-Ce/Na-Lben(CP) (b) Au/Al-Ce-Na-LBen

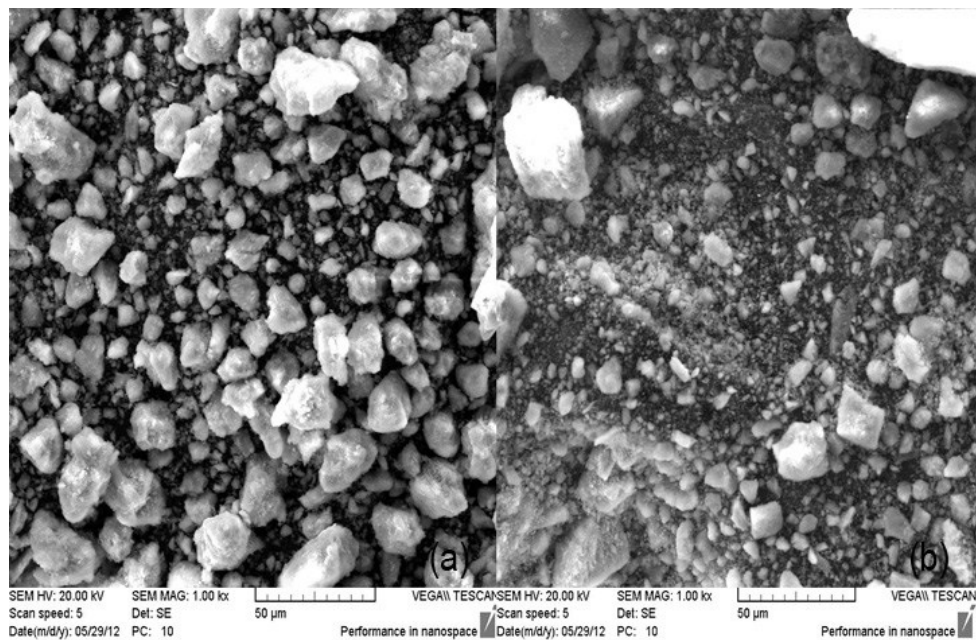


Fig. 6. FT-IR spectra of the catalysts. a. Al-Ce-Na-Lben, b. Na-Lben, c. Au-Al-Ce/Na-LBen(CP), d. Au-Al-Ce/Na-LBen(HT), e. Au/Na-Lben, f. Au/Al-Ce-Na-LBen

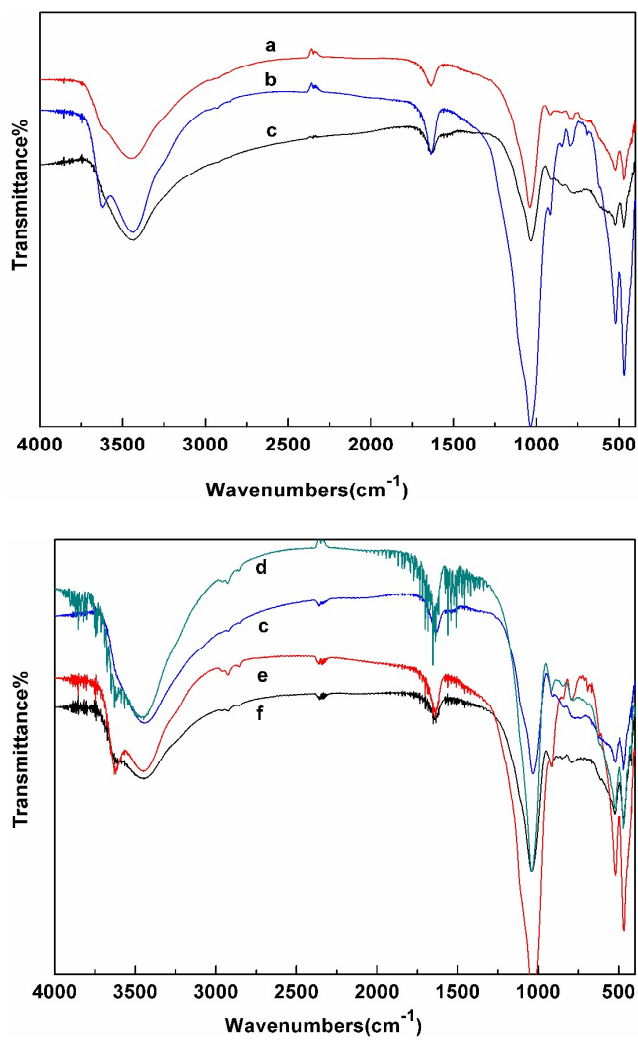


Table 1. The real contents of Au and Ce were measured by ICP and XPS

Sample	ICP		XPS	
	Au(%)	Ce(%)	Au(%)	Ce(%)
Au/Na-LBen	0.01	/	0.04	/
Au/Al-Ce-Na-LBen	0.32	0.018	0.11	3.23
Au-Al-Ce/Na-LBen(CP)	0.39	0.0087	0.18	0
Au-Al-Ce/Na-LBen(HT)	0.36	0.011	0.16	6.14

Table 2. BET surface area, pore volume and average pore size of the catalyst supports and catalysts

Sample	Average pore diameter (nm)	Pore volum(cm^3/g)	$S_{\text{BET}}(\text{m}^2/\text{g})$
Ben	6.68	0.059	35.5
LBen	4.23	0.223	210.9
Na-Ben	7.07	0.058	32.8
Na-LBen	4.61	0.177	153.8
Al-Ce-Na-LBen	9.02	0.405	179.7
Au/Al-Ce-Na-LBen	9.72	0.408	168.1
Au-Al-Ce/Na-LBen (HT)	11.6	0.449	154.1
Au-Al-Ce/Na-LBen (CP)	4.46	0.209	187.3

Graphical Abstract

